Automatic Calibration of a Single-Projector Catadioptric Display System

Benjamin Astre, Laurent Sarry
ERIM, Univ. Auvergne
BP 38, 63001 Clermont-Fd France
[astre,sarry]@u-clermont1.fr

Christophe Lohou, Eric Zeghers
LAIC, IUT, Univ. Auvergne
BP 86, 63172 Aubière France
[lohou,zeghers]@laic.u-clermont1.fr

Abstract

We describe the calibration of a catadioptric omnidirectional video-projection system that adjusts its projection to the geometry of any scene by means of a rotating camera. Correction of geometric distortions requires 3D reconstruction of the scene. A camera is used to detect projected point features and calibration is performed in three successive steps: precalibration of camera assuming pure rotation, precalibration of catadioptric projector under central approximation and calibration of the global system, by minimizing the squared distance between the reflected and perceived rays, and by relaxing previous constraints, to refine values of extrinsic parameters. Simulation is used to validate estimated values of parameters and distance between the 3D reconstruction of the projection room and its expected geometry. Influence of noise in detected point coordinates is studied and preliminary results for the reconstruction and projection in real conditions are reported.

1. Introduction

1.1. Context

We describe a novel system designed to achieve omnidirectional projection in a scene of any geometry. There are several ways to illuminate a whole room. The usual way is to use several projection channels, with one channel for each wall, each calibrated independently of the others. The main problem here lies in managing the superimposition of the channels, either using unsharp masks to obtain a fade effect between images or by photometric calibration [3]. When a single projection channel is used, optical systems must be designed to spread light in all directions: for this purpose one-channel systems often use a fish-eye lens. This expensive device produces strong radial distortions and its field of view is limited to half a space at most. Instead we propose using an optical association between a projector aimed at the room ceiling and a convex mirror placed on it. The most straightforward choice for the mirror shape is hemispheric; however, this is not the best choice from an optical point of view, as angular resolution is not homogeneous. This type of mirror has already been used to scatter light onto a dome surface in planetarium applications [2]. As the projector and mirror are never perfectly aligned, calibration is a major problem in the modeling of optical paths for projection. The main drawback of these systems is that they require laborious manual installation and that the projection is computed for a given scene geometry (dome, cave-like, etc.). We propose an automatic procedure for calibration and image mapping to any scene geometry. Although in practice most rooms are planar piecewise, the user does not have to know the exact scene layout. All that is required in order to illuminate the scene in every direction is to place the projector beneath the mirror so that the light beam covers the whole hemispheric surface.

1.2. Originality

To our knowledge, little work has been done on catadioptric projection systems [9]. Most reports have been in the context of catadioptric sensors, but the optical geometry of a catadioptric projector can be identically represented by the pinhole model. In [9], the authors propose warping the projection with specific mirrors computed for a given image to scene mapping. Our approach is on the contrary to use low cost revolution mirrors of simple shape and to infer this mapping from the scene geometry reconstructed by the system itself. Automatic scene meshing facilitates modeling operations and opens the way to mixed reality applications.

To estimate the relative position of the mirror and the catadioptric projector, an omnidirectional sensor composed of a rotating wide angle camera is used. The association of the catadioptric projector and the rotating camera has the same geometry as a hybrid stereovision device (Fig. 1).

Methods used in non central catadioptric stereovision [5] must be adapted to this particular combination. Both camera and projector are non-central: as described in section 2, the camera optical center is slightly moved away from its rotation axis, and the association of perspective optics with a hemispherical mirror is known not to possess a single view point but to present a caustic surface. A key

978-1-4244-2243-2/08/$25.00 ©2008 IEEE

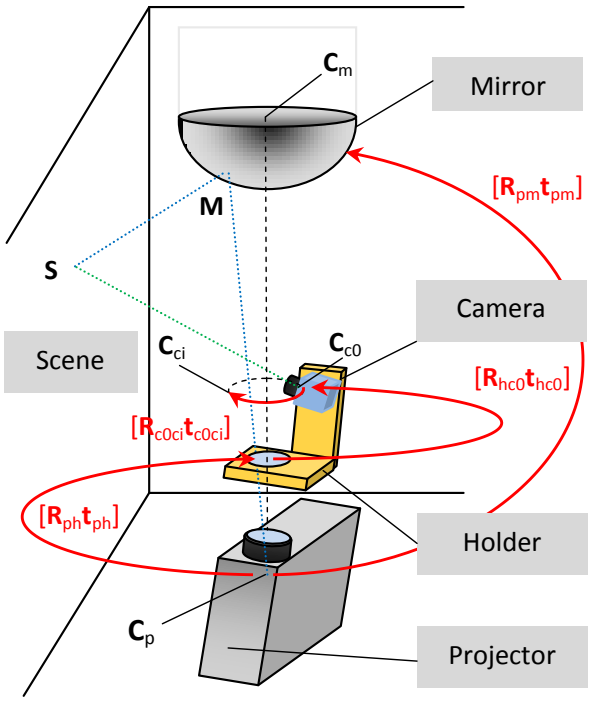

Figure 1: The system is characterized by four different coordinate systems related to the videoprojector $\Re_p$ (WCS), the mirror $\Re_m$, the camera holder $\Re_h$ and the camera at angulation i, $\Re_{ci}$. Rigid transformations have six degrees of freedom for $[\mathbf{R}_{ph}\mathbf{t}_{ph}]$, $[\mathbf{R}_{pm}\mathbf{t}_{pm}]$ and $[\mathbf{R}_{hc0}\mathbf{t}_{hc0}]$ and one degree for the rotating camera $[\mathbf{R}_{c0ci}\mathbf{t}_{c0ci}]$. The origins of these referentials are optical centers $\mathbf{C}_p$ and $\mathbf{C}_c$ and mirror center $\mathbf{C}_m$. A scene point $\mathbf{M}$ is obtained at the intersection between the projected ray reflected by the mirror and the ray incident to the camera.

point in this work is to use projected features that will be detected by the camera in an omnidirectional context. This principle is widely applied for perspective projector camera combinations, with point-like features for calibration and black and white or colored stripes for 3D object modeling, once transformations between projector and camera are known [10]. In other works, the mapping between projector and camera images handled without calibration of the projector [11,12]. It cannot be easily extended to the geometry of our projection system which is omnidirectional and non-central for both projection and acquisition, and moreover it would be impossible to generate a view point which is different from the one of the camera. In our case, points are used to compute the image-to-scene mapping by calibrating the system and reconstructing them in the world coordinates system (WCS), assumed to correspond to the projector referential. Then it is possible to create an undistorted panorama from any point of view, even if it is distant from the camera. Another advantage to know the scene geometry is that it may be used in simulation for radiometric fidelity of the projection.

Here, results of self-calibration are presented for both simulated and real projection scenes and results for 3D reconstruction are compared with the expected geometry.

2. Geometric description of the system

The self-calibrating system has four separate components: a video-projector, a hemispherical mirror, a camera and a camera holder equipped with a stepper motor. As depicted in Fig. 1, the camera is set into rotation around the optical axis of the projector: it ensures that the camera can see the whole scene with no shadow zone caused by the other components. The rotating camera itself does not mask the projector beam. It would have been more difficult to design with a catadioptric camera for instance. Also, the camera is placed as far as possible from the mirror: the angles, between rays reflected by the mirror and detected rays are at their maximum and triangulation is therefore more accurate for the reconstruction of points in 3D.

In the following, the different referentials of the system are described with rigid transformations linking them. The projector referential is considered as the world coordinate system. The angular step for camera rotation ensures approximate overlapping of half a field of view.

The hemispherical mirror used in this system is totally described by its radius r_m. For the projector and the camera the same pin-hole model can be used with perspective projection matrix $\mathbf{P}$ ($\mathbf{P}_p$ and $\mathbf{P}_c$ respectively). An image point $\tilde{\mathbf{m}}$ in homogeneous coordinates is related to a 3D point $\mathbf{M}$ by:

$$\alpha\tilde{\mathbf{m}} = \mathbf{PM} \tag{1}$$

with

$$\mathrm{P}=\begin{pmatrix} fk_u & 0 & u_0 \\ 0 & fk_v & v_0 \\ 0 & 0 & 1 \end{pmatrix} \tag{2}$$

where f is focal length (in mm), $\mathbf{m}_0 = (u_0, v_0)$ principal point (in mm) and (k_u, k_v) pixel dimension inverses (in pixels per mm). For the camera, the need for a wide angle of view (short focal length) requires taking into account radial second order distortion function f_d of center $\mathbf{c}_d$ (in mm) and coefficients k_1, k_2 [8] that relates distorted coordinates $\mathbf{m}'_c$ with undistorted ones $\mathbf{m}_c$:

$$\mathbf{m}'_c = f_d(\mathbf{m}_c) = \mathbf{m}_c + d_c\mathbf{r}_c \tag{3}$$

with

$$d_c = k_1\|\mathbf{r}_c\|^2 + k_2\|\mathbf{r}_c\|^4 \tag{4}$$

and

$$\mathbf{r}_c = \mathbf{m}_c - \mathbf{c}_d \tag{5}$$

3. Self-calibration

3.1. Principle

As the system possesses many degrees of freedom, its

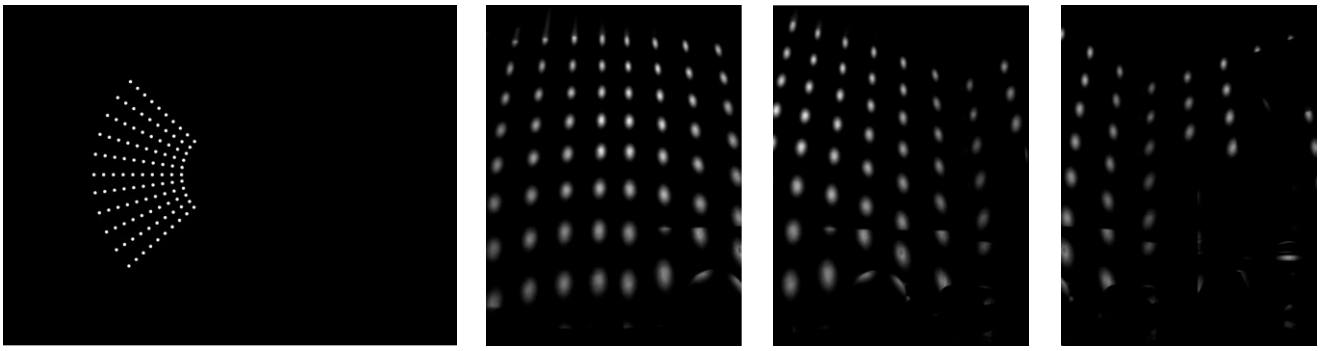

(a) **(b)** **(c)** **(d)**

Figure 2: Image of the projected point features organized as a radial mesh (a); the corresponding images acquired by the rotating camera in the first steps (b), (c), (d)... Projection is limited to the angle of view of the camera. Points are shut down one by one to pair them with camera points. A robust detection algorithm is used to compute the centers of gravity of camera points.

ease of use depends on a robust self-calibrating process. When all the transformations between components are known, light paths from the mirror and to the camera can be computed, and projected points are inferred from the intersections between them.

The user has to calibrate the system once for a given projection scene. The process must also be started over if the position of the system relative to the scene changes. The inputs of calibration are the coordinates of points in the projector matrix and their corresponding image coordinates at every camera rotation steps (Fig. 2). Some parameters, in particular the intrinsic ones, are to be specified by the user, and the others are automatically estimated.

Calibration is performed in three separate steps. The first two are precalibration steps for the rotating camera and the catadioptric projector. For the camera, the perception redundancy in rotation of projected points is used, while for the projector, methods inferred from central catadioptric sensors are used. The approximate values of parameters computed from these two initial steps are used as the initialization for a global calibration process designed to refine parameter values with no further simplifying assumptions regarding system geometry.

3.2. Approximate camera calibration

This section describes the determination of the axis of rotation, the orientation of the camera with regard to its holder and the parameters of the perspective projection and distortions.

Of these parameters, some are known from camera specifications (u_{c0}, v_{c0}, k_{cu}, k_{cv} and f_c), and others will be assumed for simplification. The angular camera rotation step is accurately known from the motor step number and the gear factor imposed by the pulleys and synchronization belt. The remaining unknowns are: $[\mathbf{R}_{hc0}\mathbf{t}_{hc0}]$, $\mathbf{c}_d$, k_1 and k_2.

The principle for the rotating camera calibration is derived from [7], but adapted to use points illuminated on the scene. Redundancy of points detected during camera rotation is used: the camera coordinates of every point detected on two successive frames are compared. For every point j and every image pair (i,i+1) the squared distance d between point $\mathbf{m}_{i+1,j}$ detected in the second image, and the point computed from the rotation of point $\mathbf{m}_{i,j}$ in the first image, is minimized to estimate the unknown parameters. All the coordinates are expressed in the camera image plane referential at angle i+1 denoted $\Re_{c_{i+1}}$:

$$d = \sum_i \sum_j \left\| f_d^{-1}(\mathbf{m'}_{i+1,j}) - \frac{z_{\mathbf{M}|\Re c_i}}{z_{\mathbf{M}|\Re c_{i+1}}} [\mathrm{R}_{c_i c_{i+1}} \mathbf{t}_{c_i c_{i+1}}] f_d^{-1}(\mathbf{m'}_{i,j}) \right\|^2 \quad (6)$$

The ratio of the depths $z_{\mathbf{M}|\Re c_i}/z_{\mathbf{M}|\Re c_{i+1}}$ of the illuminated point M with regard to the camera between angles i and i+1 is unknown unless the assumption of pure rotation is made, i.e. that the rotation axis crosses the camera optical center $\mathbf{C}_c$. This cannot be exactly true for the real system otherwise the camera itself would mask the projector light beam, but in this case, the rigid transformation is simplified to $\mathbf{R}_{c0c1}$ because the rotation axis and angle are the same for all i:

$$d = \sum_i \sum_j \left\| f_d^{-1}(\mathbf{m'}_{i+1,j}) - \mathrm{R}_{c_0 c_1} f_d^{-1}(\mathbf{m'}_{i,j}) \right\|^2 \quad (7)$$

Non-pure rotation, and the change in scale that goes with it, can be taken into account by optimizing focal length f_c as well as other parameters. The estimated value of f_c will be underestimated if the camera looks across the projector beam or otherwise overestimated. However it is discarded and replaced by the true value at the end of camera precalibration for the following steps.

The cost function (7) is minimized by means of the Levenberg-Marquardt routine LMDIF1 from MINPACK library [6].

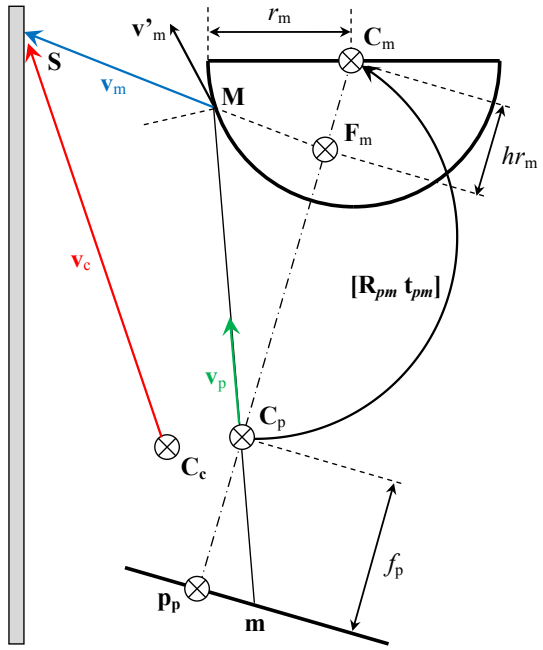

Figure 3: Simplified scheme of epipolar geometry. The reflected ray $\mathbf{v'}_m$ is changed into $\mathbf{v}_m$, collinear to $\mathbf{F}_m\mathbf{M}$, for the central assumption. It approximately holds for the rays close to projector axis of view. $\mathbf{C}_c$ is the center of the circular trajectory of the camera optical center.

3.3. Approximate calibration of the catadioptric projector

Once camera parameters are approximately known, it is possible to determine an initial configuration for the catadioptric projector. Parameters intrinsic to the projector (u_{p0}, v_{p0}, k_{pu}, k_{pv} and f_p) are known from technical specifications, as is the radius of the mirror r_m. The remaining unknowns are the extrinsic parameters relating camera holder, projector and mirror. The algorithm uses an epipolarity relationship between the rotating camera (8), assumed to be central (center $\mathbf{C}_c$) if the previous pure rotation condition holds, and the catadioptric projector (Fig. 3).

The actual shape of the mirror caustic surface in the hemispherical case is assumed to be restricted to a single focal point $\mathbf{F}_m$ located at 0.64 radius from the center (h = 0.64). In [5], this distance was shown to minimize the sum of squared angular distances between true rays coming from the mirror and rays assumed to come from the focal point (Fig. 3). The central approximation is made more accurate by the fact that rays are close to the revolution axis of the mirror, itself collinear to the projector view axis. Thus for this calibration stage, only points in the middle of the projector matrix that project onto the scene at a small height are considered.

In contrast to the method described in [5] for catadioptric stereovision, as intrinsic parameters of the camera and the catadioptric projector are known at this stage, the epipolarity constraint uses the essential matrix $\mathbf{E}$ instead of the fundamental one to relate rays coming from the mirror $\mathbf{v}_m = \mathbf{F}_m\mathbf{M}_{|\Re_m}$ and incident to the camera $\mathbf{v}_c = \mathbf{C}_c\mathbf{S}_{|\Re_{c0}}$:

$$\mathbf{v}_m^T\mathbf{E}\mathbf{v}_c = 0 \tag{8}$$

The essential matrix $\mathbf{E}$ and the translation between the projector and mirror $\mathbf{t}_{pm}$ are the unknowns at this stage. In contrast to the solution proposed in [5], where only coordinate z of $\mathbf{t}_{pm}$ was recovered, alignment of the projector with the mirror cannot be assumed because positioning is manual. Also, for our system, the height of the mirror relative to the projector can be measured with sufficient accuracy by the user. Therefore only $x_{\mathbf{t}_{pm}}$ and $y_{\mathbf{t}_{pm}}$ will be sought.

The reflected ray $\mathbf{v}_m$ is given by:

$$\mathbf{v}_m = \lambda\mathbf{v}_p + k\mathbf{t}_{pm}, \tag{9}$$

and its derivatives by:

$$\begin{cases} \dfrac{\partial\mathbf{v}_m}{\partial x_{\mathbf{t}_{pm}}} = \dfrac{\partial\lambda}{\partial x_{\mathbf{t}_{pm}}}\mathbf{v}_p - (k+1)\dfrac{x_{\mathbf{t}_{pm}}}{\|\mathbf{t}_{pm}\|^2}\mathbf{t}_{pm} + k(1\ 0\ 0)^T \\ \dfrac{\partial\mathbf{v}_m}{\partial y_{\mathbf{t}_{pm}}} = \dfrac{\partial\lambda}{\partial y_{\mathbf{t}_{pm}}}\mathbf{v}_p - (k+1)\dfrac{y_{\mathbf{t}_{pm}}}{\|\mathbf{t}_{pm}\|^2}\mathbf{t}_{pm} + k(0\ 1\ 0)^T \end{cases} \tag{10}$$

where $\mathbf{v}_p$ is the unit vector of the projected ray so that $\mathbf{C}_p\mathbf{M}_{|\Re_p} = \lambda\mathbf{v}_p$ and $k = hr_m/\|\mathbf{t}_{pm}\| - 1$.

λ and its derivatives are given by:

$$\lambda = \frac{\langle\mathbf{v}_p,\mathbf{t}_{pm}\rangle - \sqrt{\Delta}}{\|\mathbf{v}_p\|^2} \tag{11}$$

and

$$\begin{cases} \dfrac{\partial\lambda}{\partial x_{\mathbf{t}_{pm}}} = \dfrac{1}{\|\mathbf{v}_p\|^2}\left(x_{\mathbf{v}_p} - \dfrac{\partial\Delta/\partial x_{\mathbf{t}_{pm}}}{2\sqrt{\Delta}}\right) \\ \dfrac{\partial\lambda}{\partial y_{\mathbf{t}_{pm}}} = \dfrac{1}{\|\mathbf{v}_p\|^2}\left(y_{\mathbf{v}_p} - \dfrac{\partial\Delta/\partial y_{\mathbf{t}_{pm}}}{2\sqrt{\Delta}}\right) \end{cases} \tag{12}$$

with

$$\Delta = \langle\mathbf{v}_p,\mathbf{t}_{pm}\rangle^2 - \|\boldsymbol{v}_p\|^2\left(\|\boldsymbol{t}_{pm}\|^2 - {r_m}^2\right) \tag{13}$$

and

$$\begin{cases} \dfrac{\partial\Delta}{\partial x_{\mathbf{t}_{pm}}} = 2\left(\langle\mathbf{v}_p,\mathbf{t}_{pm}\rangle x_{\mathbf{v}_p} - \|\mathbf{v}_p\|^2 x_{\mathbf{t}_{pm}}\right) \\ \dfrac{\partial\Delta}{\partial y_{\mathbf{t}_{pm}}} = 2\left(\langle\mathbf{v}_p,\mathbf{t}_{pm}\rangle y_{\mathbf{v}_p} - \|\mathbf{v}_p\|^2 y_{\mathbf{t}_{pm}}\right) \end{cases} \tag{14}$$

In order to obtain a linear solution for $\mathbf{E}$ and $\mathbf{t}_{pm}$, linearization of equation (8) is performed by decomposing vector $\mathbf{v}_m$ into Taylor's series in the neighborhood of $\mathbf{t}_{pm0}$.

As stated above, instead of a linearizing with respect to $z_{\mathbf{t}_{pm}}$, it is done *vs.* $\left(x_{\mathbf{t}_{pm}}, y_{\mathbf{t}_{pm}}\right)$ to estimate relative alignment between projector and mirror:

$$\mathbf{v}_m\left(x_{\mathbf{t}_{pm}}, y_{\mathbf{t}_{pm}}\right) \approx \mathbf{v}_m(\mathbf{t}_{pm0}) + \frac{\partial\mathbf{v}_m}{\partial x_{\mathbf{t}_{pm}}}(\mathbf{t}_{pm0})\left(x_{\mathbf{t}_{pm}} - x_{\mathbf{t}_{pm0}}\right) + \frac{\partial\mathbf{v}_m}{\partial y_{\mathbf{t}_{pm}}}(\mathbf{t}_{pm0})\left(y_{\mathbf{t}_{pm}} - y_{\mathbf{t}_{pm0}}\right) \tag{15}$$

Element	Camera												Holder							Mirror		
Transformation	Distortions					Translation $\mathbf{t}_{hc0}$			Rotation $\mathbf{R}_{hc0}$				Translation $\mathbf{t}_{ph}$			Rotation $\mathbf{R}_{ph}$				Translation $\mathbf{t}_{pm}$		
Parameter	f_c	k_1	k_2	x_{cd}	y_{cd}	x	y	z	x	y	z	α	x	y	z	x	y	z	α	x	y	z
Expected	0.35	1.94	0.8	0	0	-4	0	0	0.1	0.995	0	1.343	-2	1	23.5	0.975	0.2	0.1	-0.1745	1	5	187
Initial	0.35	0	0	0	0	0	0	0	0	1	0	1.57	0	0	23.5	1	0	0	0	0	0	187
Camera precalibration	0.345	1.870	0.765	-3.77e-3	-6.344e-4				0.1	0.995	0	1.339										
Projector precalibration																0.975	0.200	0.097	-0.152	1.777	4.677	
Final calibration						-4.437	-0.154						-1.974	1.060		0.970	0.217	0.111	-0.173	0.971	4.946	

Table 1: Results for the estimation of Catopsys parameters with 520 simulated points distributed on a radial mesh, with a 5 pixel standard deviation Gaussian noise added on detected points in the camera images. Missing values are directly obtained from the previous precalibration steps. All the elements are initially slightly eccentered to simulate real conditions. All rotations are written in terms of unit quaternions.

From equations (8) and (15), we have:

$$(\mathbf{q} + \mathrm{J}(x_{\mathbf{t}_{pm}} \quad y_{\mathbf{t}_{pm}})^T)\mathrm{E}\mathbf{v}_c = 0 \tag{16}$$

with

$$\mathbf{q} = \mathbf{v}_m(\mathbf{t}_{pm0}) - \frac{\partial \mathbf{v}_m}{\partial x_{\mathbf{t}_{pm}}}(\mathbf{t}_{pm0})x_{\mathbf{t}_{pm0}} - \frac{\partial \mathbf{v}_m}{\partial y_{\mathbf{t}_{pm}}}(\mathbf{t}_{pm0})y_{\mathbf{t}_{pm0}} \tag{17}$$

and

$$\mathrm{J} = \left(\frac{\partial \mathbf{v}_m}{\partial x_{\mathbf{t}_{pm}}} \quad \frac{\partial \mathbf{v}_m}{\partial y_{\mathbf{t}_{pm}}}\right). \tag{18}$$

When the essential matrix **E** is written as a column vector **e** in row priority order, the epipolar equation (8) is equivalent to a multiparameter eigenvalue problem (MEP):

$$\left(\mathrm{D}_0 + x_{\mathbf{t}_{pm}}\mathrm{D}_1 + y_{\mathbf{t}_{pm}}\mathrm{D}_2\right)\mathbf{e} = 0 \tag{19}$$

where the j^{th} rows of matrices $\mathbf{D}_0$, $\mathbf{D}_1$ and $\mathbf{D}_2$ corresponding to the j^{th} calibration point are given by:

$$(\boldsymbol{D}_0)_j = (q_0 x_{\mathbf{v}_c j} \quad q_0 y_{\mathbf{v}_c j} \quad q_0 z_{\mathbf{v}_c j} \quad q_1 x_{\mathbf{v}_c j} \quad q_1 y_{\mathbf{v}_c j} \quad q_1 z_{\mathbf{v}_c j} \quad q_2 x_{\mathbf{v}_c j} \quad q_2 y_{\mathbf{v}_c j} \quad q_2 z_{\mathbf{v}_c j}),$$
$$(\boldsymbol{D}_1)_j = (J_{00} x_{\mathbf{v}_c j} \quad J_{00} y_{\mathbf{v}_c j} \quad J_{00} z_{\mathbf{v}_c j} \quad J_{10} x_{\mathbf{v}_c j} \quad J_{10} y_{\mathbf{v}_c j} \quad J_{10} z_{\mathbf{v}_c j} \quad J_{20} x_{\mathbf{v}_c j} \quad J_{20} y_{\mathbf{v}_c j} \quad J_{20} z_{\mathbf{v}_c j}),$$
$$(\boldsymbol{D}_2)_j = (J_{01} x_{\mathbf{v}_c j} \quad J_{01} y_{\mathbf{v}_c j} \quad J_{01} z_{\mathbf{v}_c j} \quad J_{11} x_{\mathbf{v}_c j} \quad J_{11} y_{\mathbf{v}_c j} \quad J_{11} z_{\mathbf{v}_c j} \quad J_{21} x_{\mathbf{v}_c j} \quad J_{21} y_{\mathbf{v}_c j} \quad J_{21} z_{\mathbf{v}_c j}).$$

Unlike the polynomial eigenvalue problem derived in [5], an MEP cannot be made equivalent to a generalized eigenvalue problem, as several eigenvalues must be computed. An iterative gradient descent algorithm [1] was used to solve this problem starting from guess values for **E** and $\mathbf{t}_{pm}$.

The extrinsic parameters $[\mathbf{R}_{c0m}\ \mathbf{t}_{c0m}]$ between the camera central position $\mathbf{C}_c$ and the central mirror are recovered from **E**. Direction of translation $\mathbf{t}_{cm}$ is given by the minimal singular value of **E**. Coplanarity of rows $\mathbf{e_i}$ of **E** is not ensured essentially because of the non-central assumption. Therefore, it is forced by projecting the $\mathbf{e_i}$ onto the plane normal to $\mathbf{t}_{cm}$. The rotation matrix is then given by:

$$\boldsymbol{R}_{cm} = \begin{pmatrix} \left((\boldsymbol{e}_1 \hat{} \boldsymbol{t}_{cm} + \boldsymbol{e}_2 \hat{} \boldsymbol{e}_3)/\|\boldsymbol{t}_{cm}\|^2\right)^T \\ \left((\boldsymbol{e}_2 \hat{} \boldsymbol{t}_{cm} + \boldsymbol{e}_3 \hat{} \boldsymbol{e}_1)/\|\boldsymbol{t}_{cm}\|^2\right)^T \\ \left((\boldsymbol{e}_1 \hat{} \boldsymbol{t}_{cm} + \boldsymbol{e}_2 \hat{} \boldsymbol{e}_3)/\|\boldsymbol{t}_{cm}\|^2\right)^T \end{pmatrix}. \tag{20}$$

Extrinsic parameters between the projector and the holder $[\mathbf{R}_{ph}\mathbf{t}_{ph}]$ are obtained from transformation $[\mathbf{R}_{pm}\mathbf{t}_{pm}]$, inferred from the central approximation with the estimated value for $\mathbf{t}_{pm}$, and from $\mathbf{R}_{hc0}$, approximately known from camera calibration.

3.4. Global calibration and refinement of parameters

After the two first calibrations for the rotating camera and the catadioptric projector, the purpose of the third step is to compute final values of parameters. Both pure rotation and central approximations are relaxed.

Calibration is based on the minimization of the sum of the orthogonal distances between rays reflected from the mirror $\mathbf{v'}_m$ and rays detected by the camera $\mathbf{v}_c$ (Fig. 3). It is performed for all visible projected points by means of a quasi-Newton algorithm with finite difference gradient estimation.

Not all the system parameters are optimized. Three situations are likely to occur:

- Besides intrinsic parameters of the camera and the projector, some extrinsic parameters are assumed to be measured with sufficient accuracy and will not be optimized. This is the case for the relative heights of the system components ($z_{\mathbf{t}_{pm}}$, $z_{\mathbf{t}_{ph}}$ and $z_{\mathbf{t}_{hc0}}$). Owing to the specific configuration of the system (camera rotation axis nearly merged with catadioptric projector axis $\mathbf{C}_p\mathbf{C}_m$), reflected and perceived rays still intersect when the camera holder is placed closer to the mirror. This is the natural tendency when heights are optimized. As a result, rays intersect closer to the common axis of the system and the global scale of the reconstructed points is affected. This is another reason to set height values;
- Some parameters have been estimated with sufficient accuracy by precalibration steps and will be set. Their values are often correlated with others, and they will affect convergence. This is the case for $\mathbf{R}_{hc0}$, k_1 and k_2;

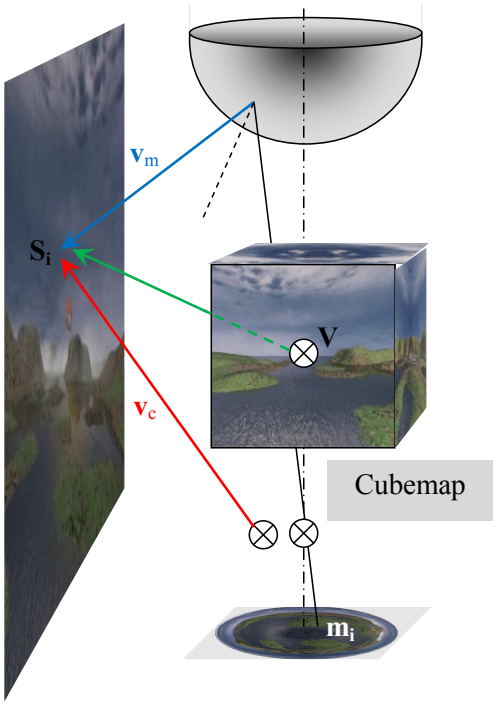

Figure 4: Principle of image-to-scene mapping for projection of a virtual content.

- Some parameters have never been optimized: $x_{t_{pm}}$, $y_{t_{pm}}$; or their values are not accurate enough after the precalibration step: $x_{t_{hco}}$, $y_{t_{hco}}$, $x_{t_{ph}}$, $y_{t_{ph}}$, and $\mathbf{R}_{ph}$ (indirectly obtained from the essential matrix **E**).

4. Image-to-scene mapping

Once the optimization of parameters is achieved, for every point $\mathbf{m}_j$ in the projector matrix, a 3D point $\mathbf{S}_j$ can be reconstructed as the closest point between rays $\mathbf{v}_m$ and $\mathbf{v}_c$, and thus it is possible to reconstruct the projection scene geometry if points structured in a mesh are projected (Fig. 4).

A viewpoint **V** is usually defined for a user standing close to the projector. Rendering of the virtual scene to be projected is performed in every direction from this viewpoint: six perspective renderings are produced simultaneously on a cubemap. Each pixel $\mathbf{m}_j$ of the projector matrix is then assigned the color of the rendering in the direction $\mathbf{VS}_i$.

5. Results and validation

5.1. Materials

The simulation environment is composed of a room of known geometry (Fig. 6(a)) about 20 square meters in area with the projection system in the middle. This is composed of a Dell 5100 MP videoprojector of resolution SXGA+ (1400×1050 pixels) at the highest focal length of the zoom interval f_p=4.6 cm, a Matrix Vision camera of resolution XGA (1024×768 pixels) with a wide angle objective of focal length f_c=3.5 mm, a 30 cm radius mirror and a 200-step motor for rotation movement.

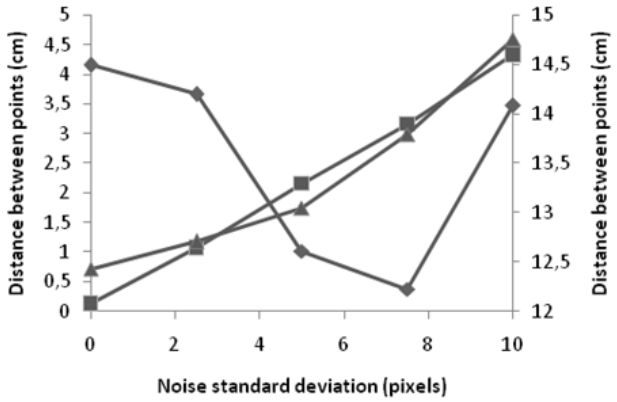

Figure 5: Distance quality indices for the reconstruction of detected points vs. standard deviation of Gaussian noise added on detected points in the camera images: distance between reflected and perceived rays after catadioptric projector precalibration (diamonds and right scale) and after final calibration (squares and left scale); mean distance between reconstructed and simulated points (triangles and left scale).

For a presentation projector like the one used here, the ordinate of the projector principal point v_{p0} is not equal to half the image plane height, because the visual axis is tilted with respect to the optical axis. It has been empirically and approximately estimated. As it has much the same effect as the inclination of the projector, there is no need to optimize it in the following.

5.2. Simulated data

The extrinsic transformations between system components are given values compatible with a manual setting. The exact optical paths from 520 points on the projector matrix to the scene are then computed, and their coordinates in the camera plane are measured for 14 images spaced every 27.2°.

Validation is performed on simulated data to compare estimated with expected values of parameters (Table 1). Results are given for a 5-pixel standard deviation Gaussian noise added to the coordinates in the image plane, which corresponds approximately to a deviation of 1.5 cm for the projected points (in the case of a wall located 2 m from the projector). In this case, precalibration steps give good initial guess values for the final refinement of parameters.

Indeed, as stated in paragraph 3.2, the value of focal length is underestimated by camera precalibration because of non-pure rotation (0.345 instead of 0.35), but distortion parameters are recovered with good accuracy. It would not have been the case if focal length was set to its true value and not optimized. Concerning precalibration of the

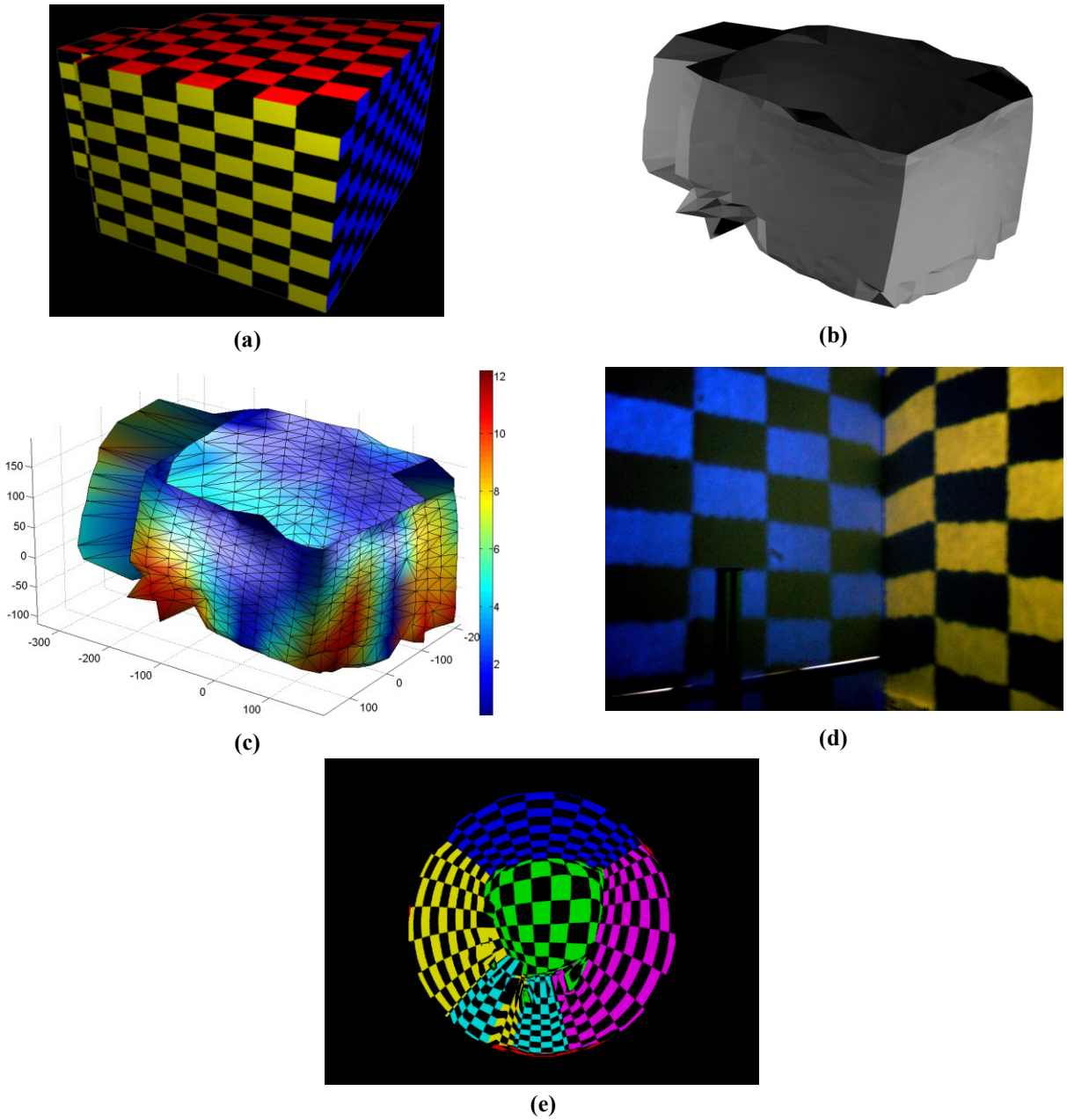

Figure 6: The virtual model of the projection room (a) is compared to the reconstructed geometry (b) with superimposition of distances (in cm) between reflected and perceived rays (c). Only the part of the room perceived by the camera is reconstructed. The virtual room is projected onto the real one using the image-to-scene mapping automatically generated from calibration (d). The corresponding projector image is given (e).

projector, table 1 reports that the axis of rotation between projector and holder is accurately recovered. In a smaller extent, this also the case for the corresponding angle and the translation vector. Their values are correctly refined by the global calibration step.

Figure 5 shows the evolution of the cost function (distance between rays) as the amount of added noise rises: precalibration performs better with noise up to a standard deviation of 8 pixels, whereas for global calibration, distance increases linearly. Distance between reconstructed points and their true simulated locations increases approximately in the same way as distance between rays.

For a standard deviation of 5 pixels, realistic with regard to the precision of point detection, an average distance of 1.75 cm to the reference points is computed.

The corresponding average distance between rays is 2.15 cm. These values are compatible with use in virtual or augmented reality.

For now, no robust operator was used in optimization algorithms. Outlier rejection could be incorporated to the camera precalibration step to make the whole calibration chain more robust to false point detections that could occur when acquisition conditions get worse (presence of stray light, reflective surfaces, etc.).

5.3. Experimental data

The true room geometry (Fig. 6(a)) has the same geometry as the previous simulated one and is experimentally reconstructed for the same projected points. Figure 6(b) shows that the reconstructed mesh has a shape visually close to the true one. Color scale (Fig. 6(c)) gives the distances between reflected and perceived rays.

For 95% of the reconstructed points, the distances lie within 8 cm. The highest distances are observed in the room corners, because vertex density is not high enough to describe edges, and at some specific locations corresponding to the presence of objects into the room (monitoring computer and desk).

Errors are globally higher than simulation mainly because of the shape of the mirror. Indeed a low cost polycarbonate mirror as the one used here is likely to deform under its own weight and thus is not perfectly hemispheric.

Nevertheless, when the virtual room of figure 6(b) is projected into the real one of figure 6(a), it is visible that distortions are satisfactorily corrected (Fig. 6(d)). In this case, the image-to-scene mapping is computed for a viewpoint located at 1.5 m above the projector center. The location and orientation of the virtual room are manually set because its initial coordinates are not expressed into the WCS attached to the projector center. The horizontal and vertical features of the projected checkerboard are preserved, except at the room corner where horizontal seem to be a bit broken. This is due to the density of vertices that is not high enough to describe strong discontinuities. We are currently working on mesh refinement based on curvature to deal with this problem.

6. Conclusion and future prospects

This self calibrating device for omnidirectional projection opens the way to immersive applications for home users. A simple autonomous calibration with no exterior phantom has been proposed. Preliminary results show good precision of 3D reconstructed points. Future works will consist in increasing robustness for various acquisition conditions. Moreover, extension to any profile of a revolution mirror is envisaged with inner estimation of shape parameters. The scatter plot obtained can be either triangulated as in this paper, or parameterized to compute the mapping between projector image and the scene. Future systems will also have the capability to map any texture onto the real scene for mixed reality purposes.

Acknowledgements

This work is funded by the Audiovisual and Multimedia Program of the French National Agency for Research (Catopsys project).

References

[1] E.K. Blum and P.B. Geltner. Numerical solution of eigentuple-eigen vector problems in Hilbert spaces by a gradient method. Numerische Mathematik, 31:231-246, 1978.

[2] P. Bourke. Spherical mirror: a new approach to hemispherical projection dome projection. Planetarian, 34(4):5-9, 2005.

[3] M. Brown, A. Majumder, and R. Yang. Camera-based calibration techniques for seamless multiprojector displays. IEEE Transactions on Visualization and Computer Graphics, 11(2):193–206, 2005.

[4] B. Micusik and T. Pajdla. Estimation of omnidirectional camera model from epipolar geometry. In Proc. IEEE CVPR, 485-490, 2003.

[5] B. Micusik and T. Pajdla. Autocalibration and 3d reconstruction with non-central catadioptric cameras. In Proc. IEEE CVPR, 58–65, 2004.

[6] J. More, B. Garbow, K. Hillstrom, User Guide for MINPACK-1,Technical Report ANL-80-74, Argonne National Laboratory, 1980.

[7] G.P. Stein. Accurate internal camera calibration using rotation, with analysis of sources of error. In Proc. ICCV, 230–236, 1995.

[8] C.C. Slama. Manual of photogrammetry, 4th edition, American Society of photogrammetry.

[9] R. Swaminathan, S. Nayar, and M. Grossberg. Framework for designing catadioptric projection and imaging systems. In Proc. IEEE International Conference on Projector-Camera Systems, 2003.

[10] G.Wang, Z. Hu, F.Wu, and H.-T. Tsui. Projector-camera based system for fast object modeling. In Proc. IEEE International Conference on Projector-Camera Systems, 2003.

[11] R. Raskar, M. S. Brown, R. Yang, W. Chen, G. Welch, H. Towles, B. Seales, and H. Fuchs, Multi-Projector Displays Using Camera-Based Registration. In Proc. IEEE Visualization, pp. 161-168, 1999.

[12] J.-P. Tardif, S. Roy, and M. Trudeau, Multi-projectors for arbitrary surfaces without explicit calibration nor reconstruction, In Proc. Conference on 3-D Digital Imaging and Modeling, pp. 217-224, 2003.